





Spatio-temporal variation of land surface temperature and temperature lapse rate over mountainous Kashmir Himalaya

Shakil Ahmad ROMSHOO*  <https://orcid.org/0000-0003-0070-5564>;  e-mail: shakilrom@kashmiruniversity.ac.in

Mohammd RAFIQ  <https://orcid.org/0000-0002-9316-8077>; e-mail: emidamls6@gmail.com

Irfan RASHID  <https://orcid.org/0000-0002-5214-1919>; e-mail: irfangis@kashmiruniversity.ac.in

* Corresponding author

Department of Earth Sciences, University of Kashmir, Hazratbal-Srinagar, 190006, Jammu and Kashmir, India

Citation: Romshoo SA, Rafiq M, Rashid I (2018) Spatio-temporal variation of land surface temperature and temperature lapse rate over mountainous Kashmir Himalaya. *Journal of Mountain Science* 15(3). <https://doi.org/10.1007/s11629-017-4566-x>

© Science Press, Institute of Mountain Hazards and Environment, CAS and Springer-Verlag GmbH Germany, part of Springer Nature 2018

Abstract: In this study, Land Surface Temperature (LST) and its lapse rate over the mountainous Kashmir Himalaya was estimated using MODIS data and correlated with the observed *in-situ* air temperature (T_{air}) data. Comparison between the MODIS LST and T_{air} showed a close agreement with the maximum error of the estimate $\pm 1^{\circ}\text{C}$ and the correlation coefficient > 0.90 . Analysis of the LST data from 2002-2012 showed an increasing trend at all the selected locations except at a site located in the southeastern part of Kashmir valley. Using the GTOPO30 DEM, MODIS LST data was used to estimate the actual temperature lapse rate (ATLR) along various transects across Kashmir Himalaya, which showed significant variations in space and time ranging from 0.3°C to 1.2°C per 100 m altitude change. This observation is at variance with the standard temperature lapse rate (STLR) of 0.65°C used universally in most of the hydrological and other land surface models. Snowmelt Runoff Model (SRM) was used to determine the efficacy of using the ATLR for simulating the stream flows in one of the glaciated and snow-covered watersheds in Kashmir. The use of ATLR in the SRM model improved the R^2 between the observed and predicted streamflows from 0.92 to 0.97.

It is hoped that the operational use of satellite-derived LST and ATLR shall improve the understanding and quantification of various processes related to climate, hydrology and ecosystem in the mountainous and data-scarce Himalaya where the use of temperature and ATLR are critical parameters for understanding various land surface and climate processes.

Keywords: MODIS; Land Surface Temperature; Lapse Rate; DEM; Snowmelt Runoff Model ; Himalaya

Introduction

Land surface temperature (LST) plays a vital role in understanding various global and regional land surface processes related to the earth system (Pitman 2003; Wan 1999). Assessment and monitoring of various land surface processes in a complex terrain, such as Himalaya, is hampered by the scanty network of hydro-meteorological observations (Romshoo et al. 2015; Rashid et al. 2015). The problem is compounded by the logistical difficulties in conducting field measurements of hydrometeorological parameters

Received: 22 June 2017

Revised: 24 October 2017

Accepted: 26 January 2018

in the precipitous terrain in order to derive a spatially representative distribution of the hydrometeorological parameters (Hachem et al. 2012; Romshoo and Rashid 2010). Remotely sensed hydrometeorological parameters are used routinely for assessing various hydrological (Koch et al. 2016; Romshoo et al. 2012; Wang et al. 2009) and climatological processes (Kumar et al. 2014; IPCC 2007; Zhang et al. 2015) at different spatial and temporal scales. Remotely sensed LST is of a major interest for a variety of environmental and ecological applications including vector-borne disease bionomics (Blum et al. 2015; Neteler 2010), biosphere processes (Field et al. 1998; Prince and Goward 1995), biogeochemical studies (Gu et al. 2007; Running et al. 2004), agricultural applications (Weng 2003; Streutkhet 2002), energy budgeting of earth (Liu et al. 2014; Diak et al. 2004) and soil-vegetation-atmosphere transfer (SVAT) models (Hu and Brunsell 2013; Mostovovoy et al. 2006).

The meteorological observations in the sparsely instrumented mountainous Himalayan regions are unable to represent the spatial heterogeneity and are therefore spatially interpolated which leads to significant errors and often produce unrepresentative spatial patterns (Willmott and Robeson 1995). The accuracy of any interpolation technique depends upon the sample density and distribution regardless of the algorithm used (Apaydin et al. 2004; Hartkamp et al. 1999). The prediction errors generally range from 1°-3° K depending on the spatial and temporal scale and the interpolation algorithm employed (Vogt et al. 1997; Anderson 2002). Also, the complexity associated with the correct estimation of T_{air} patterns increases with increased temporal resolution (Geiger 1965). Contrarily, the Earth Observing System (EOS) provides high spatial and temporal resolution surface kinetic temperatures with accuracies of 0.3°C for oceans and 1°C over land. T_{air} is estimated from LST using statistical approaches based on the regression technique (Jang et al. 2004; Zaksek and Schroedter 2009), Temperature-Vegetation Index approach (TVX), in which it is assumed that the temperature at top of the canopy cover is the same as that within the canopy (Czajkowski et al. 2000; Prihodko and Goward 1997) or the physically-based energy balance approach based on energy balance of

atmosphere (Guzinski et al. 2013; Sun 2011). It has been shown that the relationship between the observed air temperature and the remotely sensed LST is statistically significant (Benali et al. 2012; Jain et al. 2013; Qin et al. 2002). Therefore, in view of the physiographic and geomorphic setting of mountainous Kashmir Himalaya with a very sparse network of meteorological observations, high resolution satellite-derived LST maps would provide an excellent alternative for improved assessment of the land surface and atmospheric processes.

The advances in space technology during the last few decades have provided us with a rapidly increasing number of satellite platforms with better sensor capabilities that provide various physical parameters essential to study complex physical processes of the earth system (Badar et al. 2013; Jensen 2007; Romshoo et al. 2002). The MODIS (MODerate-resolution Imaging Spectroradiometer) sensor is currently the optimal choice between temporal and spatial resolution and is an excellent data source for various local and global change research studies (Ishtiaque et al. 2016; Neteler 2010). MODIS instrument was launched in 2000 as a payload on the Terra satellite and a second MODIS instrument was launched on the Aqua satellite in 2002. MODIS enhanced the performance of AVHRR by providing both, the higher spatial resolution and greater spectral resolution data (Becker et al. 2010). MODIS and AVHRR provide daily LST images with a global coverage (Anderson et al. 2012).

In absence of the actual temperature and precipitation lapse rates, it is a common practice among researchers in the mountainous Himalaya to use the standard lapse rates of the meteorological parameters to model various hydrological, climatological and glaciological processes (Adnan et al. 2016; Dar and Romshoo 2012; Romshoo et al. 2015). However, the ATLR varies with time and space and is often found way off from the STLR of -0.65°C per 100 m altitudinal change (Panday et al. 2014; Thayyen and Dimri 2014). Assessment of the ATLR from the satellite-derived LST data would, therefore, improve the quantification of the melt processes, streamflows and other land surface processes in the mountainous terrain that requires the use of ATLR (Blöschl 1991; Brubaker et al. 1996; Kattel et al. 2013).

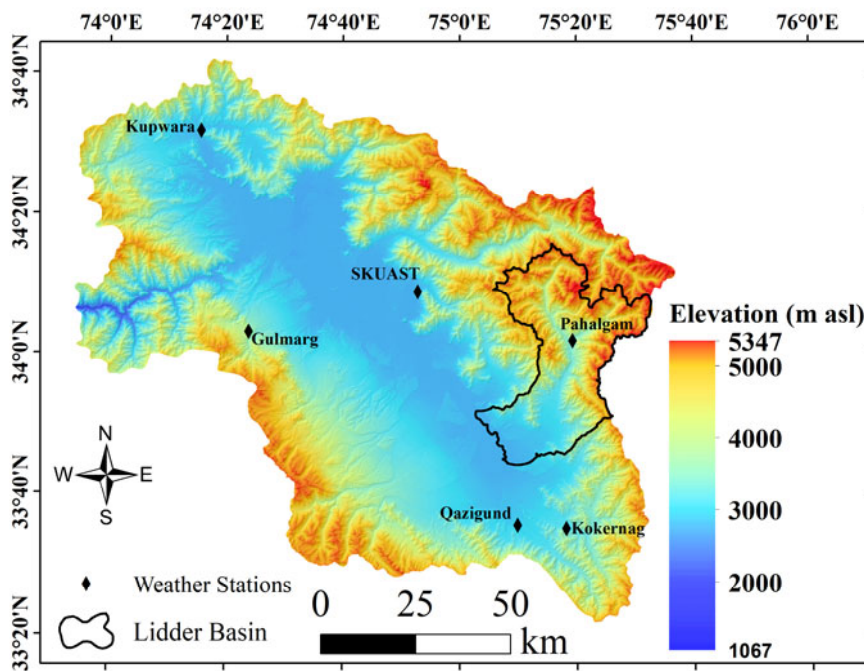


Figure 1 The study area with the location of the six meteorological stations.

1 Study Area

Kashmir valley, spread over an area of 15,534 km², is located in the vicinity of the Karakoram and western Himalayan mountain ranges (Figure 1). Kashmir valley, surrounded by the Himalayan ranges, is a longitudinal depression in the great northwestern complex of Himalayan ranges. The valley has a strong relationship with the Himalayan complex, which exercises an all-pervading influence on its geological, tectonic and geographic setting. The geomorphic setting of the Pir Panjal and the Great Himalayan range has given the Kashmir valley an oval shape with its long diagonal parallel to the general direction of the bordering mountain ranges. The maximum length of the basin, from SE-NW, is ~190 km while as the maximum width from crest of the Pir Panjal to that of the Great Himalaya is ~120 km. In altitude, it ranges from 1067 m (Uri) to a maximum of 5274 m (Kolahoi Peak).

Kashmir valley has a unique position in the Himalaya so it possesses an extensive body of evidence on the evolution of its surface features. The valley has undergone the alternations of glacial and fluvial activity corresponding to the glacial and interglacial periods during the Pleistocene

epoch (Raza et al. 1978). These processes have left indubitable imprints on the surface features of the valley (Rashid et al. 2017; Dar et al. 2017). The valley is situated in subtropical latitudes, but owing to the orographic features and snow-clad peaks, the climate over greater parts of the region resembles to that of the mountainous and continental parts of the temperate latitudes. The average winter and summer temperatures at Srinagar station range from 5°C to 25°C while the annual precipitation is 660 mm (Romshoo and Rashid 2014). However, the precipitation increases as

we move towards higher altitudes in the study area. Kashmir plains are predominantly under agricultural fields with sparse settlements, the mountainous landscapes are dominated by lush green coniferous forest, pastures and shrub lands (Rather et al. 2016). Areas above 3500 m above sea level (asl) are mostly rock exposures or under perennial snow packs and glaciers.

2 Material and Methods

2.1 Data Sets used

LST 8-day composite data at 1-km resolution, downloaded from the MODIS satellite, GTOPO30 Digital Elevation Model (DEM), observed air temperature, streamflows, snow cover and other ancillary data was used to accomplish the research objectives in this study. 11 years MODIS LST time series data (2002-2012) was processed using various image-processing techniques (Jensen 2005). The orbital configuration of the two MODIS satellites makes it possible to get the LST Terra data during day and nighttime around 10:30–12:00 A.M./P.M. local time and the LST Aqua data around 1:00–3:00 A.M./P.M. local time. The latest

MODIS LST version (V 005) used in this study has a significant improved spatial coverage, stability, and accuracy when compared with the previous versions (Wan and Dozier 1996).

The maximum air temperature (T_{air}) data, available at daily time step, from the six meteorological observatories, located in different land cover and altitude regimes (Figures 1,2, Table 1), was used to validate the satellite-derived LST data from 2002-2012. The maximum daily observed temperature was used for comparison with the satellite-derived LST as the MODIS satellite overpasses the study area at around 11:00 hrs (± 2.5 hrs) and the maximum, temperature observations centers around 11.30 AM. We also used GTOPO30 DEM with a spatial resolution of ~ 1 km for determining the ATLR over the Kashmir valley. Additionally, we used MODIS derived 8-day snow cover product with a spatial resolution of 500m resolution for removing snow covered areas in our analysis.

2.2 Methods

2.2.1 MODIS LST data processing

Medium spatial resolution satellite data are nowadays available almost real time at no cost from the MODIS satellite. In this study, an

automated method for the extraction of LST and emissivity values from the MODIS, under clear-sky conditions, was used to generate surface temperature maps (Vancutsem et al. 2010; Wan et al. 2002). The MODIS LST is derived from two thermal infrared bands (TIR) operating at 10.78–11.28 μm and 11.77–12.27 μm wavelengths. The emissivity values from these two bands are converted to LST (in K) using the algorithm given below:

$$T_s = C + (A_1 + A_2 \frac{1 - \epsilon}{\epsilon} + A_3 \frac{\Delta\epsilon}{\epsilon^2}) \frac{T_{31} + T_{32}}{2} + (B_1 + B_2 \frac{1 - \epsilon}{\epsilon} + B_3 \frac{\Delta\epsilon}{\epsilon^2}) \frac{T_{31} - T_{32}}{2} \quad (1)$$

$$\epsilon = (\epsilon_{31} + \epsilon_{32}) / 2 \quad (2)$$

$$\Delta\epsilon = \epsilon_{31} - \epsilon_{32} \quad (3)$$

where, T_s = LST, T_{31} and T_{32} are MODIS band 31 and 32 brightness temperatures; ϵ_{31} and ϵ_{32} are MODIS band 31 and 32 surface emissivities; C , A_1 , A_2 , A_3 , B_1 , B_2 and B_3 are regression coefficients.

$$T_s(k) = a_0(k) + a_1(k)T_{31} + a_2(k)T_{32} + a_3(k) (T_{31} - T_{32})^2 + a_4(k) (\sec \theta - 1) \quad (4)$$

where, a is the regression coefficient for surface types, k is the index of the surface types, and θ is

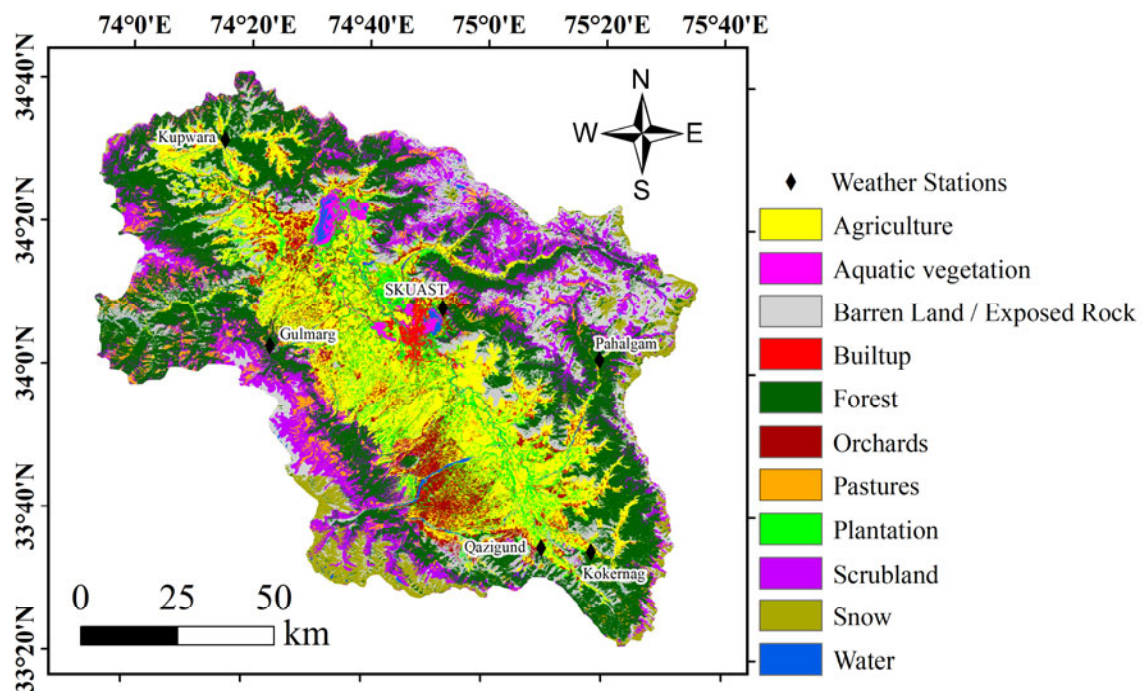


Figure 2 Land use and land cover map of Kashmir Himalaya with six meteorological stations.

Table 1 Details of meteorological stations of six meteorological observatories

Station name	Latitude	Longitude	Altitude (m)	Land cover type
Gulmarg	34° 3' 10.73" N	74° 23' 56.18" E	2660	Forest
Kokernag	33° 35' 5.23" N	75° 18' 13.89" E	1939	Built up
Kupwara	34° 31' 48.21" N	74° 15' 38.71" E	1633	Built up
Pahalgam	34° 1' 54.03" N	75° 19' 18.69" E	2185	Built up
Qazigund	33° 35' 34.15" N	75° 9' 54.48" E	1729	Built up
SKUAST	34° 8' 52.85" N	74° 52' 51.09" E	1601	Agriculture

the satellite viewing angle.

The atmospheric effects are corrected using the split-window algorithm (Wan and Dozier 1996) considering that the signal difference in the two TIR bands is caused by differential absorption of radiation in the atmosphere (Wan et al. 2002). The algorithm also corrects for emissivity effects, assuming that it is known in each ~1 km² pixel, using prior knowledge of the land cover type (Synder et al. 1998). The product aims at retrieving LST with an error less than 1°C (±0.7°C SD) in the range of -10°C to +50°C, assuming that the surface emissivity is known (Wan and Li 1997). Though, LST with errors lower than 1°C have been validated over homogeneous surfaces such as crop and grassland surfaces (Wan and Li 1997; Weng et al. 2004) but the heterogeneity of the land cover might induce larger errors in the LST. The processing of the downloaded MODIS data was accomplished in the following two steps:

Step1: Preprocessing of the satellite data involved the exclusion of LST values outside the permitted range of 220°K to 390°K. During the preprocessing, mainly the view angle, cloud cover and quality assurance aspects were checked. The images were first checked for the view angle as the view angles from 45°-69° can introduce appreciable error in the measurements of LST (Muster et al. 2015; Wan et al. 2002). Therefore, the pixels falling in this range were processed using the nearest neighborhood filtering technique (kernel size 3×3) that removes pixel outliers by substituting them with mean values of the neighboring pixels. Cloud detection and cloud masking are important preprocessing steps, because a major source of error in the retrieval of LST from thermal infrared satellite data is due to the cloud contamination (Wan 2010). Therefore, the detection and elimination of fully or partly cloudy pixels is necessary pre-processing step for the extraction of LST (Sun et al. 2005). The composite images with less than 25% cloud cover

were selected for extraction of LST. However, in case the cloud cover exceeded 25%, 8-day composite MODIS LST images were used. The nearest neighborhood filtering technique was used after cloud masking. The errors in the remotely sensed LST due to cloud cover, view angle, altitude, snow cover etc. may accumulate up to about 3 K (Wan and Snyder 2012). To correct for the errors due to snow cover, MODIS 8-day 500 m spatial resolution snow-cover data was used (Wang et al. 2008).

Step 2: During the post-processing, MODIS LST images were re-projected to the desirable projection (UTM WGS 1984 Zone 43North). The study area was extracted from the MODIS scene, which covers a larger area of 1200x1200 km. After that, the attribute information of the image data was built by multiplying each pixel value with the respective scale factor (Wan 2007). The equation used for converting pixel values (PV) into temperature (°C) is given below:

$$t = (PV \times 0.02) - 272.15 \quad (5)$$

where, t is the temperature of the pixel.

2.2.2 MODIS LST data validation

The time series of the satellite derived LST data was validated with the observed air temperature data (2002-2012). It is pertinent to mention here that the MODIS LST data is actually the temperature of land surface (skin temperature) while as the weather stations records temperatures at 2.5 m above the ground surface. To examine the statistical relationship between the measured maximum air temperature and the remotely sensed LST from MODIS, a simple linear regression method (R^2) was employed. LST from 1 km MODIS LST under clear sky conditions was correlated with the observed air temperatures on weekly, monthly, seasonal and yearly basis. The T_{air} daily data from all the six stations corresponding to the satellite derived 8-day composite LST temperature was first

averaged for 8 days, for comparison using three approaches to determine the correlation: 1) MODIS LST was compared with the T_{air} observed data for the exact location/pixel where the station is located. The locations of stations were determined using high precision GPS with an accuracy of ± 10 m, 2) the MODIS LST temperature corresponding to the 9 neighboring pixels was compared with the T_{air} observed data averaged for 8 days and 3) the best pixel among the 25 neighboring MODIS LST pixels in the vicinity of the station was compared with the observed 8-day averaged T_{air} observed data. The best pixel out of the 25 pixels was assessed manually in GIS by making a mesh of 25 points (as shapefile) each centered at the centre of the pixel. ArcMap 10.1 module, extract multi values to points function (that extracts pixel values from multiple rasters), was used to extract LST value of each pixel, which was then compared with the observed data.

2.2.3 Lapse rate and snowmelt runoff estimation

After finding good correlation between the satellite-derived LST and observed air temperature, ATLR was also estimated using the MODIS-derived LST. In GIS environment, contours from the DEM at 1 km interval were generated at 1100 m, 2100 m, 3100 m, 4100 m and 5100 m. LST variation along 8 different altitudinal transects, located across the Kashmir valley, was analyzed for determining ATLR with each transect having at least three contours. Since the mountain aspect and land cover type have significant impact on the LST (Blandford et al. 2008; Kirchner et al. 2013), it was ensured that the pixels with same aspect (derived from DEM) and land cover type were selected for estimating the ATLR along a transect.

Snowmelt runoff estimation from the glaciated basins is commonly based on the integrated use of remotely sensed data, DEM and hydrometeorological observations in a modeling framework. Snowmelt Runoff Model (SRM) is designed to simulate and forecast daily stream flow in montane basins of almost any size with elevation ranging from 305-7690 m asl, where snowmelt is a major runoff factor (Martinec 1975). The SRM model was run in the Lidder basin of the Kashmir valley to simulate the usefulness of ATLR in estimating streamflows. The overall structure of the model is described by the following equation:

$$Q_{n+1} = [c_{sn} \cdot a_n (T_n + \Delta T_n) S_n + c_{rn} P_n] \frac{A \cdot 10000}{86400} (1 - k_{n+1}) + Q_n k_{n+1} \quad (6)$$

where, Q =average daily discharge ($m^3 s$); c = runoff coefficient for snow (index sn) and rain (index rn); the degree-day factor, a , is stated as water equivalent ($cm C^{-1} d^{-1}$); T = number of degree-days ($^{\circ}C d$) which refers to the number of positive degree days (degrees above $0^{\circ}C$); ΔT =temperature lapse rate adjustment ($^{\circ}C d^{-1}$); S =ratio of the snow covered area to the total area; P =precipitation contributing to runoff (cm); A =area of the basin or zone (km^2); k =recession coefficient; n =sequence of days during the discharge computation period and $10000/86400$ = conversion from $cm km^2 d^{-1}$ to $m^3 s^{-1}$. T , S , and P are variables measured or determined each day. The runoff coefficients (C_r , C_s) take into account an estimate of evapotranspiration, sublimation of snow and ice, percolation to deep ground water from the basin. The C_r and C_s coefficients of the Jhelum basin encompassing Kashmir valley, based on calibration and validation of the four years discharge data (2007-2011), were used in the study (Sharma et al. 2012). The model was calibrated for the hydrological 2007-2008 and the validation of the simulated discharge was done using the data of 3 hydrological years (2008-2011). All the observed parameters that were input into the model were taken as initial/ base values for the calibration and then simulation was carried out for the next 3 years viz., 2008-2011. This was done to check the reliability of the calibrated values worked out for the year 2007-2008. The recession coefficient (k) indicates the decline of discharge in a period without snowmelt or rainfall. Its value ranges between 0.9 to 1 for various months and was derived from the equation:

$$k = \frac{Q_{m+1}}{Q_m} \quad (7)$$

where, m , $m+1$ are the sequence of days during a true recession flow period.

Besides, the standard temperature lapse rate of $-0.0065^{\circ}C m^{-1}$, MODIS LST based ATLR was also used to simulate snowmelt runoff. ΔT and lag time, which are characteristics for a given basin, were taken from the literature (Sharma et al. 2012). The precipitation data from the Pahalgam station was used as input for SRM. The daily mean

temperature data was extrapolated to the hypsometric mean elevation of different zones using the standard lapse rate of $-0.0065^{\circ}\text{C m}^{-1}$ and the actual lapse rate determined from the MODIS LST images. A critical temperature value is specified to determine whether the measured precipitation is rain or snow and is generally above 0°C (Charbonneau 1981). The critical temperature of 2°C was employed to distinguish snowfall and rainfall events as it has been found reliable elsewhere in the Himalayan basins (Aggarwal et al. 2014). Since the basin elevation ranges from 1500 to 5274 m, the Lidder basin was subdivided into four elevation zones. Snow depletion curves (SDC) were interpolated from the periodical snow cover maps to daily fractional snow cover values. The average daily runoff (Q) was calculated by linearly summing up the runoff contributions from each elevation zone, which were calculated separately before routing (Martinec et al. 2008; Eigdir 2003).

3 Results and Discussion

3.1 MODIS-derived LST and its validation

The average difference between the observed

and MODIS LST was within 1°C . Depending upon the approach for comparing LST with T_{air} , R^2 varied between 0.88-0.92 (Figure 3). The R^2 value between the observed temperature and LST of the exact pixel was 0.88 (Figure 3a). However, the relationship improved to 0.883 (Figure 3b) when the LST average of 9 surrounding MODIS pixels was compared with the observed temperature. The R^2 was highest (0.92) when the LST of the best of the 25 neighboring pixels in the vicinity of the station was compared with the observed temperature (Figure 3c). Generally, it was observed that the LST of the winter months (December, January and February) showed weak correlations with the observed temperature for all the stations due to the presence of extensive snow cover over the land surface (Table 2).

Trend analysis of the weekly, monthly, seasonal and annual LST data from all the six stations showed that the temperature in Kashmir Himalaya is increasing except at Qazigund (Figure 4). It was generally found that the temperature in winter months is increasing significantly during the 11-year observation period. Similar trends in the winter temperature have been reported from the region using long-term observation data (Romshoo et al. 2015; Rashid et al. 2015; Zaz and Romshoo

Table 2 Validation of the MODIS-derived Land Surface Temperature (LST) with observatories station data

Station	Average Temperature ($^{\circ}\text{C}$)		Maximum Temperature ($^{\circ}\text{C}$)		Minimum Temperature ($^{\circ}\text{C}$)		R^2
	Observed	MODIS LST	Observed	MODIS LST	Observed	MODIS LST	
Gulmarg	11.87	11.85	28	28	-5.9	-6	0.98
Kokernag	18.5	18.2	31.05	32	-1.1	-4	0.97
Kupwara	20.5	19.2	35.01	33	0.7	0	0.97
Pahalgam	17.29	16.16	28	29	-3	-3	0.95
Qazigund	19.5	19.3	30.5	32	0.01	0.1	0.95
SKUAST	19.9	20.1	34.3	35	0	-1	0.98

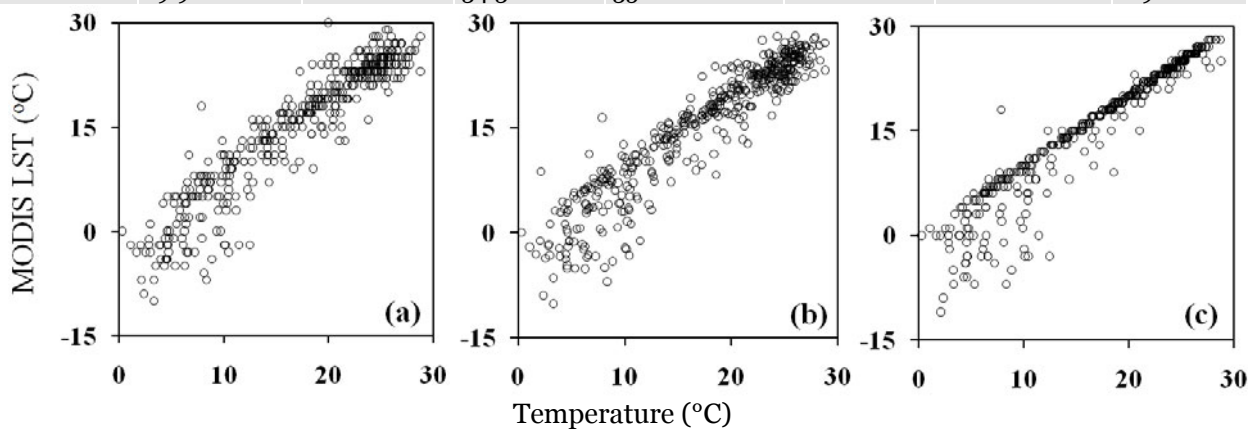


Figure 3 Validation of the MODIS-derived Land Surface Temperature (LST) with the observed T_{air} data from all the six stations; a) with the exact pixel; b) with an average of the neighboring 5×5 pixels; and c) with the best pixel in the neighboring 5×5 window.

2013). The station-wise validation of the satellite-derived LST is provided in the Table 2 and is briefly discussed below.

Comparison of the satellite-derived LST and the observed air temperature on daily basis from 2002-2012, for the six locations widely spread across the study area, is shown in the Figure 5(a-f). A close agreement was found between the two with the $R^2=0.98$ for Gulmarg (Figure 5a). Figure 5b shows the comparison of the satellite LST and observed air temperature for the Kokernag station with $R^2=0.97$. The comparison of the satellite-derived LST with the observed air temperature at Kupwara (Figure 5c) also suggests a close agreement with $R^2=0.97$. There is an error between the observed minimum temperature (0.7°C) and LST minimum temperature (0°C) during the winters. Figure 5d shows a close agreement between the observed temperature and Satellite derived LST at Pahalgam with $R^2=0.95$. The observed lowest temperatures

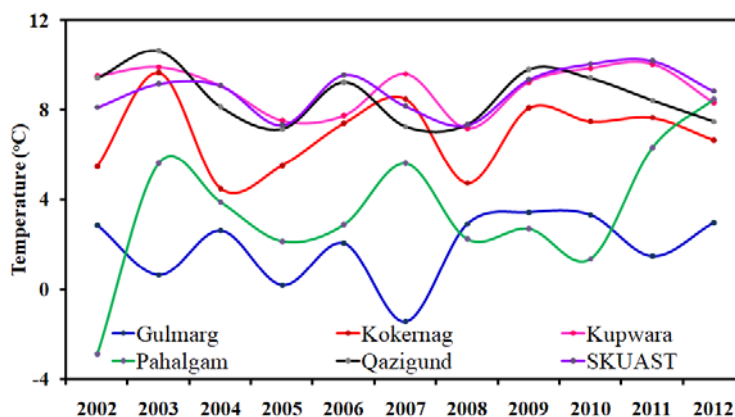


Figure 4 Temporal variation of the MODIS-derived Land Surface Temperature (LST) at six locations from 2002-2012.

and MODIS derived LST were found same. The correlation of the time series satellite-derived LST of Qazigund (Figure 5e) yielded a close agreement with $R^2=0.95$ with the winter LST showing large disagreement. The time series of the satellite-derived LST for the SKUAST station was compared with the observed air temperature at SKUAST (Figure 5f) and a close agreement was found between the two with $R^2=0.98$. The observed

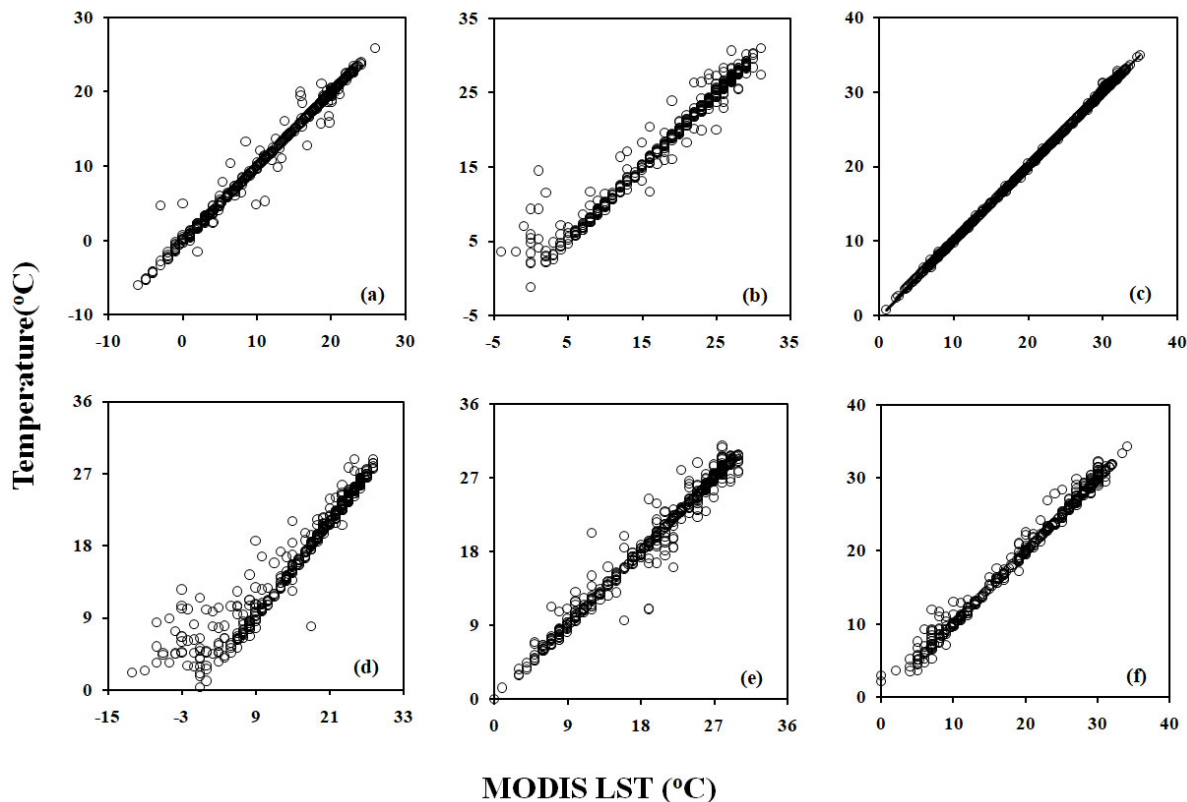


Figure 5 Correlation of the Land Surface Temperature (LST) with the observed air temperature at six observed stations; a) Gulmarg; b) Kokernag; c) Kupwara; d) Pahalgam; e) Qazigund; and f) SKUAST.

lowest winter temperature was 0°C and the corresponding MODIS LST was -1°C for the station (Table 2) showing a weak correlation.

3.2 Importance of ATLR for estimating snow- and glacier-melt

3.2.1 MODIS LST-based lapse rate

The altitudinal variability of LST-derived ATLR along 6 different transects across the Kashmir valley (Figure 6), covering at least 3 contours (2100-5100 m) is shown in Figure 7. Transect along Uri has a gradient from 1100-3100 m and the Pahalgam transect crosses the three altitudinal gradients from 2100-5100 m asl. The rest of the transects cross the altitudinal gradient from 2100-4100 only. If and when there are more than two places falling in the same altitudinal transect, the temperature lapse rate variation was shown as minimum, maximum and average (Figure 7b, c). The analysis of the data shown in the Figure 7 (a-d) shows that the temperature lapse rate varies in space and time along different

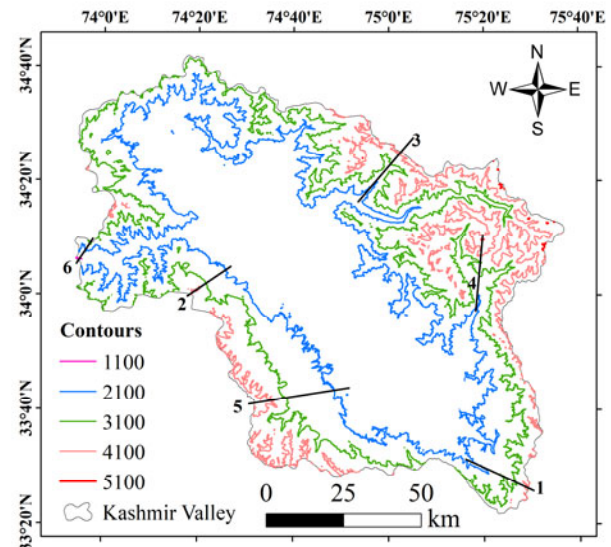


Figure 6 Location of various temperature lapse rate transects chosen across different altitudes from 1100-5100 m asl in the Kashmir valley.

transects due to the variable environmental setting (from 0.3°C -1.2°C per 100 m) against the STLR of 0.65°C per 100 m change in altitude used

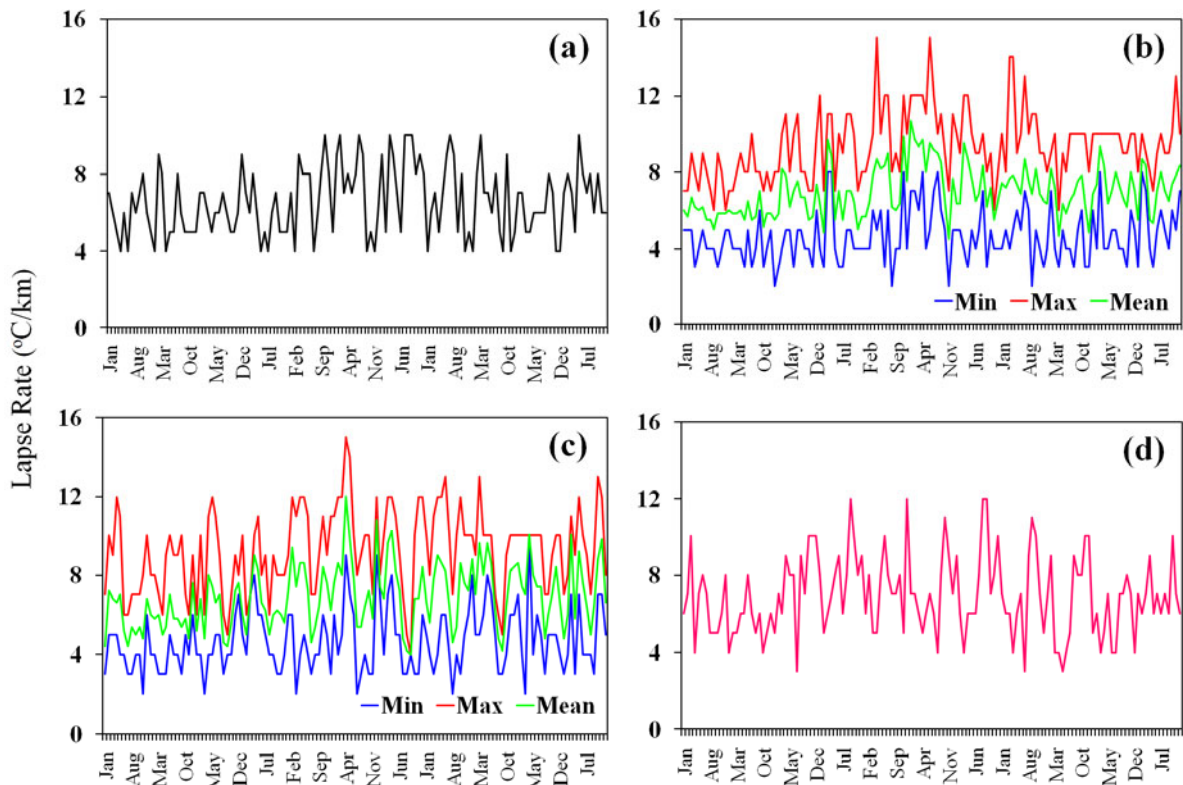


Figure 7 Altitudinal variability of LST-derived actual temperature lapse rate (ATLR) along different transects in the Kashmir valley (from 0.3°C -1.2°C per 100 m); a) Uri (transect 6) having gradient from 1100-3100 b) Bandipora and Pahalgam (transect 3 and 4) having altitudinal gradients from 2100-5100 m asl; c) Banihal and Shopian (transect 1 and 5) having altitudinal gradients from 2100-5100 m asl; and d) Baramulla (transect 2) having the altitudinal gradient from 2100-4100 only.

universally. The variation in lapse rate is a function of season, atmospheric conditions (stability of atmospheric column vis-a-vis temperature inversion), climate and land cover (Li et al. 2013). In the Lidder valley, it was found that the ATLR is higher in the altitudinal range of 3100-<4100 m than along the 2100-<3100 m and 4100-<5100 m altitude gradients (Figure 8). The overall lapse rate from 2100-<5100 m in the Lidder valley is 7.1°C km⁻¹, which is 0.6°C higher than the STLR. Also, the weekly and monthly trends of the temperature lapse rate were analyzed which showed that the lapse rate is not uniform and varies with time and altitudinal gradient (Figure 8). The temperature lapse rate can go up as high as 12°C km⁻¹ and can stay as low as 3°C km⁻¹. Overall, the temperature lapse rate is higher along the 3100-<4100 m altitudinal gradient compared to the 2100-<3100 m gradient (Table 3).

3.2.2 Temperature lapse rate and snowmelt runoff modeling

The use of the STLR, in absence of the ATLR, in modeling the glacio-hydrological processes often leads to inaccurate stream flow estimates in the mountainous region. In order to demonstrate the usefulness of using the ATLR for snowmelt estimation in the mountainous Lidder catchment, Kashmir valley, SRM was used to estimate and compare the snowmelt runoff using the ATLR and the STLR. Figure 9 shows comparison of the actual hydrograph with the simulated hydrographs using the ATLR and STLR. The overall correlation between the measured and simulated discharge is high indicating that the calibrated parameters closely fit the real-world situation. However, there are a few minor disagreements as well particularly during 2010-2011 hydrological year. It is evident from the results that the use of the ATLR improves the estimation of the streamflow compared to the estimates using the STLR. The correlation coefficient between the observed and simulated streamflow improved from 0.92 for STLR to 0.97 for the ATLR in Lidder. However, keeping in view

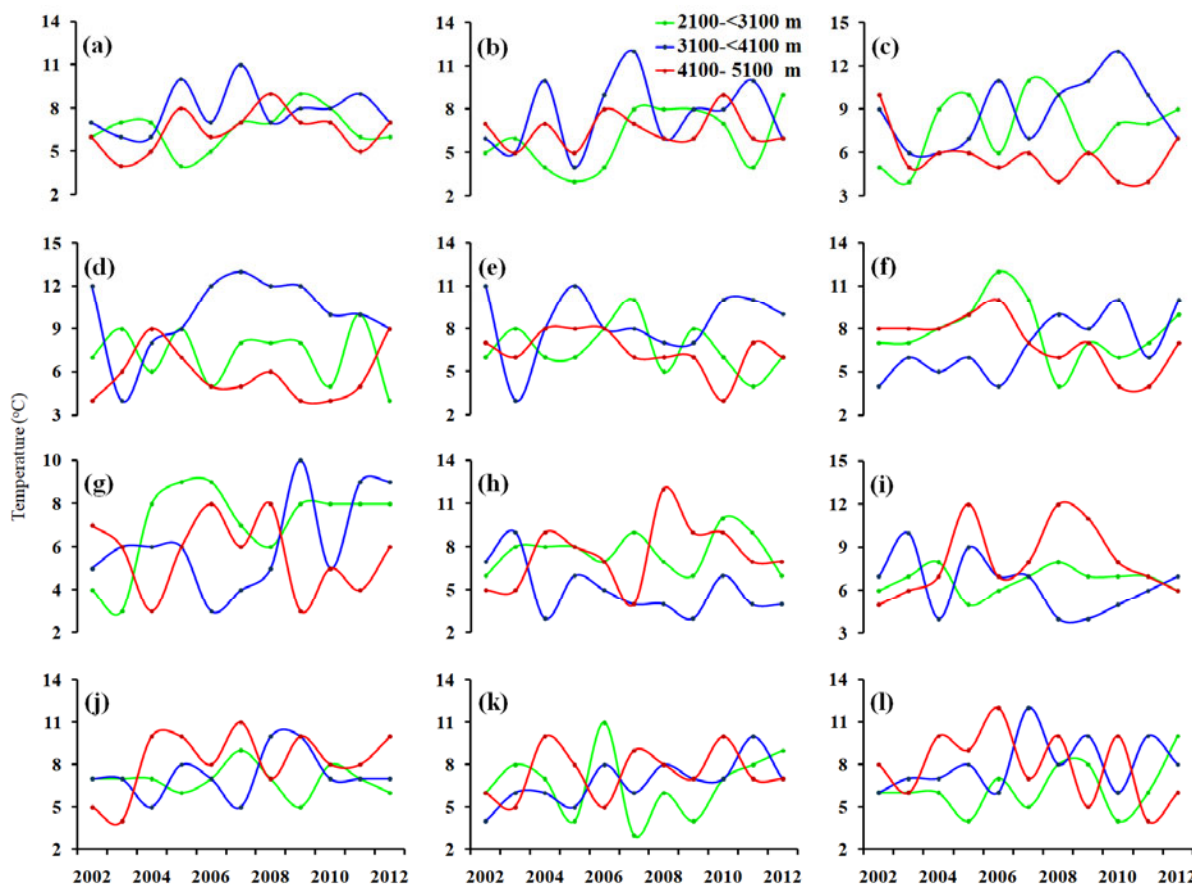


Figure 8 Temporal altitudinal variability of actual temperature lapse rate (ATLR) in Lidder valley, Kashmir from 2100-5100m amsl from January to December.

Table 3 Altitude range wise lapse rate as determined from MODIS LST data

Month	Altitude Range (m asl)		
	2100-<3100	3100-<4100	4100-<5100
Jan	6.5	8.4	6.4
Feb	6	8.5	6.5
Mar	7.4	8.5	5.7
Apr	7	8.5	5.7
May	6.6	8.7	6.7
Jun	7.4	6.8	7.4
Jul	7.4	6	6.5
Aug	7.5	5.7	6.7
Sep	7	7	8
Oct	7	7.4	8.3
Nov	7	6.6	7.3
Dec	6.5	7.7	8.7
Average	6.94 (± 0.46)	7.48 (± 1.06)	6.99 (± 0.97)

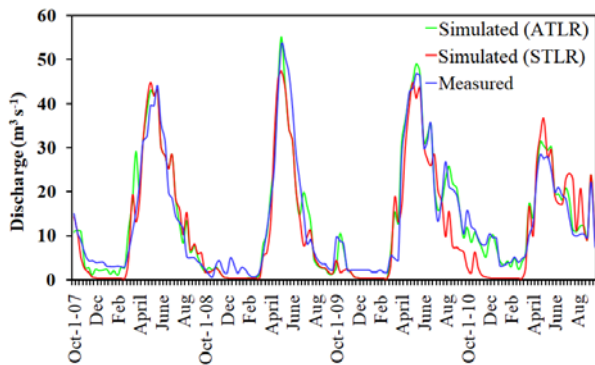


Figure 9 Comparison of the observed hydrograph with the two simulated hydrographs using the actual temperature lapse rate (ATLR) and standard temperature lapse rate (STLR).

the fact that there could be sometimes a large difference in the STLR and ATLR as observed elsewhere in the Kashmir valley, it is prudent to use the satellite-derived LST for estimating the temperature lapse rates for use in the glacio-hydrological models for accurate snow-melt estimates in the ungauged mountainous catchments. Further, there is a need to validate the improvements reported in the glacier- and snow-melt using the ATLR in this research by using other glacio-hydrological models based on energy balance or degree day approach (Arnold et al. 1996; Braithwaite and Raper 2007; Datt et al. 2008).

3.3 Importance of satellite derived temperature lapse rate in Himalaya

Using the temperature observations from just 4 meteorological stations in Kashmir Himalaya,

Zaz and Romshoo (2013) estimated the temperature lapse rates varying from $-3.89^{\circ}\text{C km}^{-1}$ to $4.96^{\circ}\text{C km}^{-1}$ which have high uncertainty due to the inadequate number of observation stations used in the estimation of the temperature lapse rate. Similar variations in the temperature lapse rate ($-4.8^{\circ}\text{C km}^{-1}$ to $-7.6^{\circ}\text{C km}^{-1}$) were reported by Tahir et al. (2011) in the Karakoram region, again based on a few meteorological observatories. Thayyen et al. (2014) reported the temperature lapse rate of $-2.8^{\circ}\text{C km}^{-1}$ to $-17.0^{\circ}\text{C km}^{-1}$ for the cold arid region of Ladakh Himalaya and $-1.9^{\circ}\text{C km}^{-1}$ to $-9.0^{\circ}\text{C km}^{-1}$ for monsoon dominated Garhwal region in the Western Himalaya based on the few observed temperatures along a transect. The temperature lapse rates determined from the MODIS LST data in this study, based on 1-km resolution data, varied between $-3.0^{\circ}\text{C km}^{-1}$ to $12.0^{\circ}\text{C km}^{-1}$ due to the changes in the seasons, topography, land cover and climatic setting. It is believed that, instead of using the STLR of $-6.5^{\circ}\text{C km}^{-1}$ altitudinal change, the findings would go a long way in the operational use of the satellite-derived temperature lapse rates for quantifying various hydrological and glaciological processes in the mountainous Himalaya.

4 Conclusion

In this research, a time series of MODIS satellite data was used for extracting the LST which was validated with the observed air temperature (weekly, monthly, seasonally and yearly time scales) from six meteorological stations in the Kashmir Himalaya. The analysis indicated statistically significant agreement, with $R^2 > 90\%$, between the satellite-derived LST and the observed air temperature. However, despite correction for the snow-cover, the satellite-derived LST showed some errors during winters. The findings provide confidence for the use of satellite-derived LST in mountainous Himalaya where the understanding and modeling of various land surface and atmospheric processes related to hydrology, climatology and glaciology is constrained due to lack of adequate observed meteorological data. However, it is important to validate the LST with observed data from adequate number of observatories to check its suitability for use in the process models. Further in the data-scarce regions,

use of the standard temperature lapse rate of $6.5^{\circ}\text{C km}^{-1}$ in glacio-hydrological models is often erroneous and might significantly affect the quantification of snow-melt and ice-melt in snow-covered and glaciated regions like Himalaya. It was found that the ATLR varies significantly with time and space as compared to the constant STLR. Using the Snowmelt Runoff Model, it was observed that the use of the ATLR improved the estimation of streamflows ($r=0.97$) compared to estimates using the STLR ($r=0.92$). The satellite-derived LST has a good potential to replace the use of STLR in various land surface and atmospheric process models to improve the quantification of various land and atmospheric processes in the mountainous regions.

References

- Adnan M, Nabi G, Poomee MS, Ashraf A (2016) Snowmelt runoff prediction under changing climate in the Himalayan Cryosphere: a case of Gilgit River Basin. *Geoscience Frontiers*. <https://doi.org/10.1016/j.gsf.2016.08.008>
- Anderson MC, Allen RG, Morse A, Kustas WP (2012) Use of Landsat thermal imagery in monitoring evapotranspiration and managing water resources. *Remote Sensing of Environment* 122:50-65. <https://doi.org/10.1016/j.rse.2011.08.025>
- Anderson S (2002) An evaluation of spatial interpolation methods on air temperature in Phoenix, AZ. Available online: <http://www.cobblestoneconcepts.com/ucgis2summer/anderson/anderson.htm>, accessed on 1 November 2015.
- Apaydin H, Sonmez FK, Yildirim YE (2004) Spatial interpolation techniques for climate data in the GAP region in Turkey. *Climate Research* 28(1):31-40. <http://doi.org/10.3354/cro28031>
- Arnold NS, Willis IC, Sharp MJ, et al. (1996) A distributed surface energy-balance model for a small valley glacier. *Journal of Glaciology* 42(140): 77-89. <https://doi.org/10.3189/S0022143000030549>
- Badar B, Romshoo SA, Khan MA (2013) Modelling the catchment hydrological response in a Himalayan lake as a function of changing land system. *Earth System Science* 112(2): 434-450. <https://doi.org/10.1007/s12040-013-0285-z>
- Becker-Reshef I, Vermote E, Lindeman M, Justice C (2010) A generalized regression-based model for forecasting winter wheat yields in Kansas and Ukraine using MODIS data. *Remote Sensing of Environment* 114(6): 1312-1323. <https://doi.org/10.1016/j.rse.2010.01.010>
- Benali A, Carvalho AC, Nunes JP, et al. (2012) Estimating air surface temperature in Portugal using MODIS LST data. *Remote Sensing of Environment* 124: 108-121. <https://doi.org/10.1016/j.rse.2012.04.024>
- Blandford TR, Humes KS, Harshburger BJ, et al. (2008) Seasonal and synoptic variations in near-surface air temperature lapse rates in a mountainous basin. *Journal of Applied Meteorology and Climatology* 47(1): 249-261. <https://doi.org/10.1175/2007JAMC1565.1>
- Blöschl G (1991) The influence of uncertainty in the air temperature and albedo on snowmelt. *Hydrology Research* 22: 95-108.
- Blum M, Lensky IM, Rempoulakis P, Nestel D (2015) Modeling insect population fluctuations with satellite land surface temperature. *Ecological Modelling* 311: 39-47. <https://doi.org/10.1016/j.ecolmodel.2015.05.005>
- Braithwaite RJ, Raper SCB (2007) Glaciological conditions in seven contrasting regions estimated with the degree-day model. *Annals of Glaciology* 46: 297-302. <https://doi.org/10.3189/172756407782871206>
- Brubaker K, Rango A, Kustas W (1996) Incorporating radiation inputs into the Snowmelt Runoff Model. *Hydrological Processes* 10: 1329-1343. [https://doi.org/10.1002/\(SICI\)1099-1085\(199610\)10:10<1329::AID-HYP464>3.0.CO;2-W](https://doi.org/10.1002/(SICI)1099-1085(199610)10:10<1329::AID-HYP464>3.0.CO;2-W)
- Chow V T, Maidment DR, Mays LW (1988) *Applied hydrology*. McGraw-Hill Series in Water Resources and Environmental Engineering. McGraw-Hill: New York. ISBN 0-07-010810-2.
- Czajkowski KP, Goward SN, Stadler S, Walz A (2000) Thermal remote sensing of near surface environmental variables: Application over the Oklahoma Mesonet. *The Professional Geographer* 52(2): 345-357. <https://doi.org/10.1111/0033-0124.00230>
- Dar RA, Romshoo SA (2012) Estimating daily stream flow from the glacierized mountainous Kashmir Himalayan basin. *Journal of Research and Development* 12: 113-130. Available online: <http://cord.uok.edu.in/Files/4701b853-a330-4f94-a00e-01555a32a0ff/Journal/9ef27cc3-2512-4ef9-95c5-2ee0a8a936e7.pdf>, accessed on 1 October 2017.
- Dar RA, Paul, O, Murtaza, KO, Romshoo, SA (2017). Glacial-geomorphic study of the Thajwas glacier valley, Kashmir Himalayas, India. *Quaternary International*, 444: 157-171. <https://doi.org/10.1016/j.quaint.2017.05.021>
- Datt P, Srivastava PK, Negi PS, Satyawali PK (2008) Surface energy balance of seasonal snow cover for snow-melt estimation in N-W Himalaya. *Journal of Earth System Science* 117(5): 567-573. <https://doi.org/10.1007/s12040-008-0053-7>
- Diak GR, Mecikalski JR, Anderson MC, et al. (2004) Estimating land surface energy budgets from space: Review and current efforts at the University of Wisconsin-Madison and USDA-ARS. *Bulletin of the American Meteorological Society* 85(1): 65-78. <https://doi.org/10.1175/BAMS-85-1-65>
- Egdir AN (2003) Investigation of the snowmelt runoff in the Orumiyeh region, using modeling, GIS and RS techniques. M.Sc. thesis, Enschede, Netherlands, International Institute for Geoinformation Science and Earth Observation (ITC). Accessed online: https://www.itc.nl/library/papers_2003/msc/wrem/Najafi.pdf, accessed on 1 November 2016.

Acknowledgements

The work was conducted as part of the Department of Science and Technology (DST), Government of India sponsored consortium project titled “Himalayan Cryosphere: Science and Society” and the financial assistance received from the Department under the project to accomplish this research is thankfully acknowledged. The authors express gratitude to the three anonymous reviewers and the handling Editor for their valuable comments and suggestions on the earlier versions of the manuscript that have greatly improved the content and structure of the manuscript.

- Field CB, Behrenfeld MJ, Randerson JT, Falkowski P (1998) Primary production of the biosphere: integrating terrestrial and oceanic components. *Science* 281(5374): 237-240. <https://doi.org/10.1126/science.281.5374.237>
- Geiger R (1965) *The Climate near the ground*. Fourth Edition. Cambridge, MA: Harvard University Press.
- Gu L, Meyers T, Pallardy SG, et al. (2007) Influences of biomass heat and biochemical energy storages on the land surface fluxes and radiative temperature. *Journal of Geophysical Research: Atmospheres* 112(D2). <https://doi.org/10.1029/2006JD007425>
- Guzinski R, Anderson MC, Kustas WP, et al. (2013) Using a thermal-based two source energy balance model with time-differencing to estimate surface energy fluxes with day-night MODIS observations. *Hydrology and Earth System Sciences* 17(7): 2809-2825. <https://doi.org/10.5194/hess-17-2809-2013>
- Hachem S, Duguay CR, Allard M (2012) Comparison of MODIS-derived land surface temperatures with ground surface and air temperature measurements in continuous permafrost terrain. *The Cryosphere* 6(1): 51-69. <https://doi.org/10.5194/tc-6-51-2012>
- Hartkamp AD, De Beurs K, Stein A, White JW (1999) Interpolation techniques for climate variables. NRG-GIS Series 99-01. Mexico, D.F.: CIMMYT. ISSN: 1405-7484. Available online: <http://repository.cimmyt.org:8080/xmlui/bitstream/handle/10883/988/67882.pdf?sequence=1>, accessed on 1 November 2016.
- Hu L, Brunsell NA (2013) The impact of temporal aggregation of land surface temperature data for surface urban heat island (SUHI) monitoring. *Remote Sensing of Environment* 134: 162-174. <https://doi.org/10.1016/j.rse.2013.02.022>
- Huete A, Didan K, Miura T, et al. (2002) Overview of the radiometric and biophysical performance of the MODIS vegetation indices. *Remote Sensing of Environment* 83(1): 195-213. [https://doi.org/10.1016/S0034-4257\(02\)00096-2](https://doi.org/10.1016/S0034-4257(02)00096-2)
- IPCC (2007) *Climate Change 2007: The Physical Science Basis. Contribution of Working Group I to the Fourth Assessment Report of the Intergovernmental Panel on Climate Change*. In: Solomon S, Qin D, Manning M, et al. (eds.), Cambridge, United Kingdom: Cambridge University Press.
- Ishtiaque A, Myint SW, Wang C (2016) Examining the ecosystem health and sustainability of the world's largest mangrove forest using multi-temporal MODIS products. *Science of The Total Environment* 569: 1241-1254. <https://doi.org/10.1016/j.scitotenv.2016.06.200>
- Jain SK, Goswami A, Saraf AK (2013) Determination of land surface temperature and its lapse rate in the Satluj River basin using NOAA data. *International Journal of Remote Sensing* 29(11): 3091-3103. <https://doi.org/10.1080/01431160701468992>
- Jang JD, Viau AA, Ancil F (2004) Neural network estimation of air temperatures from AVHRR data. *International Journal of Remote Sensing* 25: 4541-4554. <https://doi.org/10.1080/01431160310001657533>
- Jensen JR (2005) *Introductory digital image processing: A remote sensing perspective* (III Edition). Prentice-Hall Inc. ISBN: 0131453610
- Jensen JR (2007) *Remote sensing of the environment: An earth resource perspective* (II Edition). Prentice-Hall Inc. ISBN: 97881731716809
- Kattel DB, Yao T, Yang K, et al. (2013) Temperature lapse rate in complex mountain terrain on the southern slope of the central Himalayas. *Theoretical and Applied Climatology* 113(3-4): 671-682. <https://doi.org/10.1007/s00704-012-0816-6>
- Kirchner M, Faus-Kessler T, Jakobi G, et al. (2013) Altitudinal temperature lapse rates in an Alpine valley: trends and the influence of season and weather patterns. *International Journal of Climatology* 33(3): 539-555. <https://doi.org/10.1002/joc.3444>
- Koch J, Siemann A, Stisen S, Sheffield J (2016) Spatial validation of large - scale land surface models against monthly land surface temperature patterns using innovative performance metrics. *Journal of Geophysical Research: Atmospheres* 121(10): 5430-5452. <https://doi.org/10.1002/2015JD024482>
- König M, Winther JG, Isaksson E (2001) Measuring snow and glacier ice properties from satellite. *Reviews of Geophysics* 39(1): 1-27. <https://doi.org/10.1029/1999RG000076>
- Kumar R, Singh S, Randhawa SS, et al. (2014) Temperature trend analysis in the glacier region of Naradu Valley, Himachal Himalaya, India. *Comptes Rendus Geoscience* 346(9): 213-222. <https://doi.org/10.1016/j.crte.2014.09.001>
- Li X, Wang L, Chen D, et al. (2013) Near - surface air temperature lapse rates in the mainland China during 1962-2011. *Journal of Geophysical Research: Atmospheres* 118(14): 7505-7515. <https://doi.org/10.1002/jgrd.50553>
- Liu YQ, Mamtimin A, Huo W, et al. (2014) Estimation of the land surface emissivity in the hinterland of Taklimakan Desert. *Journal of Mountain Science* 11(6): 1543-1551. <https://doi.org/10.1007/s11629-014-3090-5>
- Lulla K, Helfert M, Holland D (1994) The NASA Space Shuttle Earth Observations database for global change science. In *Remote Sensing and Global Climate Change* (pp. 355-365). Springer Berlin Heidelberg. https://doi.org/10.1007/978-3-642-79287-8_16
- Martinez J (1975) Snowmelt-runoff model for stream flow forecasts. *Hydrology Research* 6(3): 145-154.
- Mostovoy GV, King RL, Reddy KR, et al. (2006) Statistical estimation of daily maximum and minimum air temperatures from MODIS LST data over the state of Mississippi. *GIScience & Remote Sensing* 43(1): 78-110. <https://doi.org/10.2747/1548-1603.43.1.78>
- Muster S, Langer M, Abnizova A, et al. (2015) Spatio-temporal sensitivity of MODIS land surface temperature anomalies indicates high potential for large-scale land cover change detection in Arctic permafrost landscapes. *Remote Sensing of Environment* 168: 1-12. <https://doi.org/10.1016/j.rse.2015.06.017>
- Neteler M (2010) Estimating daily Land Surface Temperatures in mountainous environments by reconstructed MODIS LST data. *Remote Sensing* 2(1): 333-351. <https://doi.org/10.3390/rs1020333>
- Panday PK, Williams CA, Frey KE, Brown ME (2014) Application and evaluation of a snowmelt runoff model in the Tamor River basin, Eastern Himalaya using a Markov Chain Monte Carlo (MCMC) data assimilation approach. *Hydrological Processes* 28(21): 5337-5353. <https://doi.org/10.1002/hyp.10005>
- Pitman AJ (2003) The evolution of, and revolution in, land surface schemes designed for climate models. *International Journal of Climatology* 23: 479-510. <https://doi.org/10.1002/joc.893>
- Prihodko L, Goward SN (1997) Estimation of air temperature from remotely sensed surface observations. *Remote Sensing of Environment* 60(3): 335-346. [https://doi.org/10.1016/S0034-4257\(96\)00216-7](https://doi.org/10.1016/S0034-4257(96)00216-7)
- Prince SD, Goward SN (1995) Global primary production: a remote sensing approach. *Journal of Biogeography* 22: 815-835. <https://doi.org/10.2307/2845983>
- Qin Z, Karnieli A, Berliner P (2002) Remote sensing analysis of the land surface temperature anomaly in the sand-dune region across the Israel-Egypt border. *International Journal of Remote Sensing* 23(19): 3991-4018. <https://doi.org/10.1080/01431160110116310>
- Rashid I, Romshoo SA, Abdullah T (2017) The recent deglaciation of Kolahoi valley in Kashmir Himalaya, India in response to the changing climate. *Journal of Asian Earth Sciences* 138: 38-50. <https://doi.org/10.1016/j.jseas.2017.02.002>
- Rashid I, Romshoo SA, Chaturvedi RK, et al. (2015) Projected Climate Change Impacts on Vegetation Distribution over Kashmir Himalayas. *Climatic Change* 132(4): 601-613. <https://doi.org/10.1007/s10584-015-1456-5>

- Rather MI, Rashid I, Shahi N, et al. (2016) Massive land system changes impact water quality of the Jhelum River in Kashmir Himalaya. *Environmental Monitoring and Assessment* 188(3): 1-20. <https://doi.org/10.1007/s10661-016-5190-x>
- Raza M, Ahmad A, Mohammad A (1978) *The Valley of Kashmir: A Geographical Interpretation*. Vikas Publishing House: New Delhi. ISBN: 9780890890585
- Romshoo SA, Bhat SA, Rashid I (2012) Geoinformatics for assessing the morphometric control on the hydrological response at watershed scale in Upper Indus basin. *Earth System Science* 121(3): 659-686. <https://doi.org/10.1007/s12040-012-0192-8>
- Romshoo SA, Dar RA, Rashid I, et al. (2015) Implications of shrinking cryosphere under changing climate on the streamflows in the Lidder catchment in the Upper Indus Basin, India. *Arctic Antarctic and Alpine Research* 47(4): 627-644. <https://doi.org/10.1657/AAAR0014-088>
- Romshoo SA, Koike M, Hironaka S, et al. (2002) Influence of Surface and Vegetation Characteristics on C-band Radar Measurements for Soil Moisture Content. *Journal of Indian Society of Remote Sensing* 30(4): 229-244. <https://doi.org/10.1007/BF03000366>
- Romshoo SA, Rashid I (2010) Potential and Constraints of Geospatial Data for Precise Assessment of the Impacts of Climate Change at Landscape Level. *International Journal of Geomatics and Geosciences* 1(3), 386-405. Available online: <http://www.ipublishing.co.in/jggsvol1n012010/EIJGGS2009.pdf>, accessed on 1 November 2016.
- Running SW, Nemani RR, Heinsch FA, et al. (2004) A continuous satellite-derived measure of global terrestrial primary production. *Bioscience* 54(6): 547-560. [https://doi.org/10.1641/0006-3568\(2004\)054\[0547:ACSMO G\]2.0.CO;2](https://doi.org/10.1641/0006-3568(2004)054[0547:ACSMO G]2.0.CO;2)
- Sharma V, Mishra VD, Joshi PK (2012) Snow cover variation and streamflow simulation in a snow-fed river basin of the Northwest Himalaya. *Journal of Mountain Science* 9(6): 853-868. <https://doi.org/10.1007/s11629-012-2419-1>
- Singh P (1991) A temperature lapse rate study in western Himalayas. *Hydrology Journal (Indian Association of Hydrologists)* 14: 156-163.
- Snyder W, Wan Z, Zhang Y, Feng YZ (1998) Classification-based emissivity for land surface temperature measurement from space. *International Journal of Remote Sensing* 19: 2753-2774. <https://doi.org/10.1080/014311698214497>
- Streutker DR (2002) A remote sensing study of the urban heat island of Houston, Texas. *International Journal of Remote Sensing* 23(13): 2595-2608. <https://doi.org/10.1080/01431160110115023>
- Sun Y (2011) Retrieval and application of land surface temperature Available online: <http://www.geo.utexas.edu/courses/387h/papers/term%20paper-sun.pdf>, accessed on 1 November 2016.
- Sun YJ, Wang JF, Zhang RH, et al. (2005) Air temperature retrieval from remote sensing data based on thermodynamics. *Theoretical and Applied Climatology* 80(1): 37-48. <https://doi.org/10.1007/s00704-004-0079-y>
- Tahir AA, Chevallier P, Arnaud Y, et al. (2011) Modeling snowmelt-runoff under climate scenarios in the Hunza River basin, Karakoram Range, Northern Pakistan. *Journal of Hydrology* 409(1): 104-117. <https://doi.org/10.1016/j.jhydrol.2011.08.035>
- Thayyen RJ, Dimri AP (2014) Factors controlling Slope Environmental Lapse Rate (SELR) of temperature in the monsoon and cold-arid glacio-hydrological regimes of the Himalaya. *The Cryosphere Discussions* 8(6): 5645-5686. <https://doi.org/10.5194/tcd-8-5645-2014>
- Vancutsem C, Ceccato P, Dinku T, Connor SJ (2010) Evaluation of MODIS land surface temperature data to estimate air temperature in different ecosystems over Africa. *Remote Sensing of Environment* 114(2): 449-465. <https://doi.org/10.1016/j.rse.2009.10.002>
- Vogt JV, Viau AA, Paquet F (1997) Mapping regional air temperature fields using satellite - derived surface skin temperatures. *International Journal of Climatology* 17(14): 1559-1579. [https://doi.org/10.1002/\(SICI\)1097-0088\(19971130\)17:14<1559::AID-JOC211>3.0.CO;2-5](https://doi.org/10.1002/(SICI)1097-0088(19971130)17:14<1559::AID-JOC211>3.0.CO;2-5)
- Wan Z (1999) MODIS land-surface temperature algorithm theoretical basis document (LST ATBD). Institute for Computational Earth System Science, Santa Barbara, 75. Available online: https://modis.gsfc.nasa.gov/data/atbd/atbd_mod11.pdf, accessed on 1 November 2016.
- Wan Z (2006) MODIS land surface temperature products users' guide. Institute for Computational Earth System Science, University of California, Santa Barbara. Available online: <http://citeseerx.ist.psu.edu/viewdoc/download?doi=10.1.1.457.2833&rep=rep1&type=pdf>, accessed on 1 November 2016.
- Wan Z (2007) Collection-5 MODIS Land Surface Temperature Products Users' Guide. ICESSE, University of California, Santa Barbara. Available online: http://www.icesse.ucsb.edu/modis/LstUsrGuide/MODIS_LST_products_Users_guide_C5.pdf, accessed on 1 November 2016.
- Wan Z, Dozier J (1996) A generalized split-window algorithm for retrieving land-surface temperature from space. *IEEE Transactions on Geoscience and Remote Sensing* 34(4): 892-905. <https://doi.org/10.1109/36.508406>
- Wan Z, Li ZL (1997) A physics-based algorithm for retrieving land-surface emissivity and temperature from EOS/MODIS data. *IEEE Transactions on Geoscience and Remote Sensing* 35: 980-996. <https://doi.org/10.1109/36.602541>
- Wan Z, Snyder W (2012) MODIS land-surface temperature algorithm theoretical basis document (LST ATBD). Version 3.3. Available online: https://modis.gsfc.nasa.gov/data/atbd/atbd_mod11.pdf, accessed on 1 November 2016.
- Wan Z, Zhang Y, Zhang Q, Li ZL (2002) Validation of the land-surface temperature products retrieved from Terra Moderate Resolution Imaging Spectroradiometer data. *Remote Sensing of Environment* 83(1): 163-180. [https://doi.org/10.1016/S0034-4257\(02\)00093-7](https://doi.org/10.1016/S0034-4257(02)00093-7)
- Wang W, Liang S, Meyers T (2008) Validating MODIS land surface temperature products using long-term nighttime ground measurements. *Remote Sensing of Environment* 112(3): 623-635. <https://doi.org/10.1016/j.rse.2007.05.024>
- Weiss M, Troufleau D, Baret F, et al. (2001) Coupling canopy functioning and radiative transfer models for remote sensing data assimilation. *Agricultural and Forest Meteorology* 108(2): 113-128. [https://doi.org/10.1016/S0168-1923\(01\)00234-9](https://doi.org/10.1016/S0168-1923(01)00234-9)
- Weng Q (2003) Fractal analysis of satellite-detected urban heat island effect. *Photogrammetric Engineering and Remote Sensing* 69(5): 555-566. <https://doi.org/10.14358/PERS.69.5.555>
- Weng Q, Lu D, Schubring J (2004) Estimation of land surface temperature-vegetation abundance relationship for urban heat island studies. *Remote Sensing of Environment* 89(4): 467-483. <https://doi.org/10.1016/j.rse.2003.11.005>
- Willmott CJ, Robeson SM (1995) Climatologically aided interpolation (CAI) of terrestrial air temperature. *International Journal of Climatology* 15(2): 221-229. <https://doi.org/10.1002/joc.3370150207>
- Zakšek K, Schroedter-Homscheidt M (2009) Parameterization of air temperature in high temporal and spatial resolution from a combination of the SEVIRI and MODIS instruments. *ISPRS Journal of Photogrammetry and Remote Sensing* 64(4): 414-421. <https://doi.org/10.1016/j.isprsjprs.2009.02.006>
- Zaz S, Romshoo SA (2013) Recent Variation of Temperature, Trends in Kashmir Valley (India). *Journal of Himalayan Ecology & Sustainable Development* 8: 42-63. Available online: <http://envirsc.uok.edu.in/Files/ab1ac1fi-07e3-42a2-85bc-83717ef39155/Journal/co12e6c6-7355-4afi-8950-54f718b61828.pdf>, accessed on 1 October 2017.
- Zhang X, Hu Y, Jia G, et al. (2015) Land surface temperature shaped by urban fractions in megacity region. *Theoretical and Applied Climatology* 127(3): 965-975. <https://doi.org/10.1007/s00704-015-1683-8>